Journal of Sol-Gel Science and Technology 34, 23–39, 2005

Influence of Film Structure and Precursor Composition on Rhodamine B Retention in Dye-Dopped Ormosils

VIOLETA I. URICANU*
University of Twente, Applied Physics Department/NCV, Postbus 217, 7500 AE Enschede, Netherlands
v.i.uricanu@utwente.nl

DAN DONESCU, ANDREI G. BANU AND SEVER SERBAN
Institute of Chemical Research, Splaiul Independentei 202, 77208, Bucharest, Romania

MARILENA VASILESCU
Physical Chemistry Institute of the Romanian Academy, Splaiul Independentei 202, 77208–Bucharest, Romania

MIHAELA OLTEANU AND MANUELA DUDAU
University of Bucharest, Physical Chemistry Department, 4-12 Regina Elisabeta Blvd., 70346, Bucharest, Romania

Received July 15, 2003; Accepted October 22, 2004

Abstract. The interplay between the chemical structure of the precursors, internal organization in the end materials and dye retention was investigated for composites (ormosils) doped with rhodamine B. Besides formulations with *tri*ethoxysilanes (RTES) only, we synthesized as well organic–inorganic hybrids with addition of titanium isopropoxide (TIP) and maleic anhydride (MA). The organic (R) functionality of RTES was changed from methyl (MeTES), to phenyl (PTES) and octyl (OTES). Atomic force microscopy and electron microscopy, coupled with thermogravimetric analysis prove that hydrophobicity increase stimulates the transition of film structure: from well-defined, compact particles (for MeTES), to a mixture of porous particles and non-granular material (for MeTES/PTES), with extreme results observed for octyl-based composites. For this latter, the apparent homogeneity comes from cluster-like organization, where the primary entities are *'pseudo—granules'* produced by hydrophobic interactions of oligomeric siloxanes. Controlling the composition and gelation procedure resulted in doped composites with good optical transparency and rhodamine B fluorescence emission bands at around 580 nm. Dye transport inside the inorganic structure is not facilitated when: (a) the particles have a compact (nonporous) inner structure and (b) the recipe does not contain the TIP/MA combination. For silica-based films, the dye is located in the macropores (between the granules) of the material and could be easy removed by washing with acetone. On the contrary, using TIP/MA changes not only the internal composition of the granular-like material (by creating a microporous titania-rich outer-shell of the particles) but also the affinity of the Rh-B to permeate and reside inside these new structures.

Keywords: ormosils, dye retention, atomic force microscopy (AFM), thermogravimetric analysis (TGA)

*To whom all correspondence should be addressed.

Introduction

The use of dyes in sol–gel processes attracts an increased interest due to potential applications at industrial scale, for nonlinear optical materials, optical waveguides, solid state lasers, sensors and light concentrators in solar cells [1–9]. The inorganic and dye components can be mixed at the nanometric scale, leading to the so-called hybrid organic-inorganic (nano)composites. Properties tuning for these materials can be achieved by changing the ratio and/or chemical nature of the reactants as well as the preparation conditions [10]. Besides a high versatility of the synthesis itself, the resulting materials have all the advantages of sol–gel glasses: high dye dispersion, mechanical robustness, transparency of the matrix in the visible to UV range, high processibility, etc.

Organic-inorganic composites with embedded hydrophobic domains can be prepared if the precursor of the inorganic matrix has at least one organic functionality, i.e., alkyl, alkenyl or aryl moiety. Theoretically, hydrophobic dyes will have a high retention yield in the thus created hydrophobe cages and specific dye-environment interactions [11–20] will affect the optical activity of the entrapped (dye) molecules. Compared with hydrophobic dyes, rhodamine B (Rh-B) has a reasonable good solubility in water (0.78%), alcohol (1.47%) and other polar environments. Up to date, Rh-B has been already used in sol–gel reactions with ethoxysilane compounds [21–25]. High longevity and very good photophysical properties were proved for Rh-B in the SiO_2 cage created by the sol–gel conversion of the tetraethoxysilane (TEOS) monomer in acidic conditions [22]. Also, the preparation method (doping the dye inside the sol *versus* impregnation of it in the already dried glassy material) was inspected from the point of view of material performances in time. Changes in the fluorescence intensity [23] and lasing effects [24] were studied for Rh-B doped films dried from sols with combined silicium–titanium alkoxysilanes.

As general requirements, in solid state dye lasers, the efficiency and photostability are the most important quality parameters. For such application, the main problem to be solved is the photodegradation which limits the life time of the dye and decreases the laser's efficiency after a number of exciting pulses. The photochemical stability of the entrapped dyes depends not only on the dye but also on the chemical properties of the host matrix. In a recent paper, Yang et al. [26] underlined that: "improved photostability of the dye within solid hosts has been attributed to caging and immobilizing the dye molecules, thereby preventing excited-state interaction with other species. So in a solid host, the photodegradation of the laser dye depends on the nature of dye molecule, the composition and structure of the host, and the impurities presented in the host. In order to further improve the photostability and decrease photodegradation of the laser dye, *to control the trapped surroundings of the dye molecules becomes the most critical issue for the solid-state dye laser*."

In line with these statements, our main issue in the present paper was the investigation of the roles played by the matrix structure and enrichment with hydrophobic moieties (or even hydrophobe nanodomains) on rhodamine B incorporation and retention in mixed organic-inorganic (ormosil) films. As starting precursors, different *tri*ethoxysilanes (RTES) were chosen, having a variable organic (R) functionality. Besides film preparation with RTES (as pure RTES or as combination of two RTES compounds) and Rh-B, we synthesized as well organic–inorganic hybrids following a slightly modified recipe, with addition of titanium isopropoxide (TIP). Due to the high reactivity of TIP in sol–gel conditions (as compared with the RTES), maleic anhydride (MA) was added as complexing/ retardant agent.

Atomic force microscopy and electron microscopy studies were supplemented with thermal stability, wettability and absorption/fluorescence spectral analyses. Based on the results of these combined micro- and macro-scale investigations, it was possible to observe the internal structure of the films and explain the measured properties.

Experimental

Materials

The alkoxysilanes: methyltriethoxysilane (MeTES), phenyltriethoxysilane (PTES) and octyltriethoxysilane (OTES), all products from Merck Schuchard, tetraisopropyl orthotitanate (TIP) from FlukaAG and rhodamine B (A.R.) were used without further purification. Glycerol, ethylene glycol and α-bromnaphtalene (all Sigma products) were used as received. Ethanol (Chimopar, Romania) was purified by rectification. Maleic anhydride (MA) (Reagent) was purified by sublimation.

Table 1. Alkoxysilane (RTES), titanium isopropoxide (TIP) and maleic anhydride (MA) amounts used for preparation of hybrid films. A short index is used to identify every final material.

Film index	RTES type	amount (g)	TIP (g)	MA (g)
H-Me	MeTES	2.25	–	–
H-Me-P	MeTES/PTES	1.125/1.5	–	–
H-Me-O	MeTES/OTES	1.125/2.0	–	–
H-Me-TIP	MeTES	2.25	0.2	0.038
H-Me-P-TIP	MeTES/PTES	1.125/1.5	0.2	0.038
H-Me-O-TIP	MeTES/OTES	1.125/2.0	0.2	0.038

Film Preparation

Different *tri*ethoxysilanes (RTES), titanium isopropoxide (TIP) and maleic anhydride (MA) were used as starting materials, according to the amounts in Table 1. The organic (R) functionality of the RTES was chosen such as to give more or less hydrophobicity, increasing from methyl (MeTES), to phenyl (PTES) and octyl (OTES). When TIP was incorporated in the recipe, the hybrids were prepared by a *two-step* method because TIP hydrolyzes at a much higher rate than the RTES. Thus, in all preparations, RTES was prehydrolyzed in acidic conditions with ethanol (1.25 g) and water (0.142 g) for 2 h under continuous stirring. As a second step, the TIP and maleic anydride were added to the solution, together with the second portion of water (0.3 g). The mixture was stirred for another 2 h after which the dye (rhodamine B, 0.2 ml ethanolic solution) was added to the reactant solution and stirred for another 30 min. The concentration was calculated as to give a 6.6 $\times 10^{-4}$ mol dye per mol of silicium derivate. For comparison purposes, non-doped hybrids (i.e., glass sols without dye) were prepared following identical recipes (as in Table 1).

Independent on dye presence, all final sols were homogeneous and fluid. For AFM and wettability investigations, thin films were deposited on glass slides (precleaned with piranha, repeatedly washed with water, EtOH and dried under nitrogen) by dip-coating. The slides were left further to dry at room temperature (25°C), under a mild nitrogen stream, for 2 weeks. No macroscopic cracks (i.e., visible with eye resolution) were observed after drying. The thickness of the films, the profile and the extent of thickness variation along the film surface were measured with a profilometer (Talystep Taylor Hobson). All the final films had a thickness of $\approx$30 μm. For the TGA analysis, well-determined amounts from all formulations were deposited on poly(ethylene) sheets and dried in similar conditions (as the other samples). Before measurements, the polymer substrate was peeled off, yielding self-standing composite films.

Methods

TEM and cryo-TEM measurements were done on few samples prior to gelation. Small amounts from the initial liquid sols were deposited on copper grids. Depending on the experiment type, the aforementioned copper grids were handled differently: either dried in controlled environment (for TEM), either vitrificated according with the procedure described in what follows. For the cryo-TEM experiments, the grid was mounted on a hammer-type device (driven by a pneumatic cylinder under photoelectric barrier control) and was slowly dipped into liquid nitrogen. Afterwards, the grid was transferred to the cryo-TEM holder (Gatan) with the help of a special transfer unit. With this method it was made sure that the frozen sample does not come into contact with the surrounding air and was always kept at the temperature of liquid nitrogen. Further, the as-prepared samples were observed in the conventional TEM mode of an analytical electron microscope (JEOL 2000FX).

A home-built instrument [27] (Twente University, The Netherlands) was used to observe the structure (height profile) at the film/air interface. The microscope was operated in *constant force* imaging mode at a setpoint control force of 5 nN in air. Also, the interaction between the AFM tip of the cantilever and the hybrid was measured in air with the instrument operated in the *force_versus_distance* mode. The silicon nitride cantilever (Park Scientific Instruments, with a nominal spring constant 0.1 N m^{-1}), was driven up and down at a frequency of 1 Hz. Prior to these measurements, the sensitivity of the laser—detection system on the used cantilever was determined via calibration scans on a hard substrate.

Wettability studies were conducted according to the liquid—solid contact angle method. A tiny drop (from a liquid with known properties) is gently deposited on the solid surface of the film and the contact angle is measured during a time interval of several seconds. The image of the drop profile is recorded by video enhanced microscopy. The volume of the liquid droplets (poured with a Hamilton syringe) was around 3–5 μl. Four liquids for which the surface tension components,

i.e., the Lifshitz-van der Waals (γ_L^{LW}) and acid-base (γ_L^+ and γ_L^-) contributions are known [28], were used for wetting experiments. The contact angles of these liquids with the film surfaces were measured at 20°C. The used liquids were: water (W), glycerol (G), ethylene glycol (EG) and α-bromonaphtalene (BN). The components of surface energy of solid films are the simultaneous solutions of three complete Young equations [29]:

$$\gamma_L(\cos\theta + 1) = 2\left(\gamma_L^{LW}\gamma_S^{LW}\right)^{1/2} + 2(\gamma_L^+\gamma_S^-)^{1/2} + 2(\gamma_L^-\gamma_S^+)^{1/2} \quad (1)$$

obtained for three liquids. In Eq. (1), γ_S^{LW}, γ_S^+ *and* γ_S^- are the unknown Lifshitz and acid-base components of surface energy of hybrid films.

Thermogravimetric analysis (TGA) of all samples has been carried out at a heating rate of 20°C min^{-1} in air using a Du Pont 2000 instrument. A Carl Zeiss Specord instrument was used to record the absorption spectra. Fluorescence emission spectra were recorded with a Perkin Elmer 204 spectrophotometer equipped with a 150 W xenon lamp as the excitation source ($\lambda_{excitation} = 360$ nm).

The FTIR spectra were obtained using a Nicolet 5DXC. Powdered (ormosil) samples were ground with dried KBr, pelletised and analysed immediately. The chamber of the spectrophotometer was purged with dried air. The spectra were recorded with a resolution 2–4 cm^{-1} (2000 scans).

Results and Discussions

Before presenting the data obtained by us, it is worthwise to mention few results reported by others [30–32] on pure inorganic materials prepared according to recipes only slightly different from ours. Using nitrogen adsorption studies, Montes and co-workers [30] proved that "micromesoporous" structures can by obtained by base (NH_4OH)-catalyzed hydrolysis-condensation of teraethoxysilane (TEOS) followed by reaction with Ti isopropoxide (TIP). The sample thus prepared had more than half of its surface area in large pores (equivalent diameter $\approx$ 50 nm) and 10% of its pore volume in micropores. Transmission electron microscopy and IR spectroscopy confirmed a uniform coverage of the SiO_2 particles by the TiO_2, with a part of the titania being grafted (via Ti–O–Si linkages) to the silica, while the rest was organized in small anatase aggregates. Almeida and Christensen [31] have used micro-Raman spectrometry to investigate anatase formation in powders based on TEOS/TIP recipes. For the lowest TiO_2/SiO_2 ratio used (i.e., 20/80), only heat treatment at 1000°C for at least half hour gives a volume fraction of crystallized material (anatase) above the detection limit of the experimental technique. The higher the titania content, the higher the heat treatment temperature or the longer the time allocated for it, the larger is the crystallized fraction (of the inorganic film) and the crystallite size.

Titania (small) particle segregation at the contact points between silica spheres was observed by Khalil et al. [32]. Combined TGA/DSC studies showed that no crystalline products were formed upon calcination at 600°C. However, an exothermic DSC peak was detected at 480°C and considered as indication for an aggregation process: heat treatment favors the aggregation of small titania particles into bigger ones.

For the *tri*ethoxysilanes used in the present work, the hydrophobic moiety could eventually retard the hydrolysis/condensation reaction involved in the silica network formation. Long or bulky organic functionalities cannot be easy accommodated in the growing inorganic matrix. Hence, changing the nature of the hydrophobe group implies that at the moment of TIP addition, the Si–O–Si network will have advanced up to different yields and the titania compound will react with more or less developed precursors of the end materials. Later incorporation of the Rh-B does not change the internal structure of the TiO_2/SiO_2 species, but rather takes advantage of it for dye retention.

In order to overcome the uncertainties regarding: (1) the degree of completion for the sol–gel reaction in the end materials and (2) the internal structure of these ormosil films, several techniques were used, as presented in the following sections.

Atomic Force Microscopy and Electron Microscopy Data

Imaging (*contact mode AFM*) and *force_versus_distance* scans were performed on the film surface as obtained after drying and, also, on 'washed' films. The latter ones were obtained by flushing (in controlled conditions) the films' surface with water, followed by acetone and, finally redrying at room temperature. Depending on composition, the samples' integrity suffered more or less; the changes

Table 2. The general appearance of the composite films after washing with water/acetone. The color index is defined as the intensity ratio of the transmission peaks (in visible) of the washed over the initial (nonwashed) film. Due to the modifications suffered by the material during washing, no accurate estimates of the color index can be done for wH-Me-P-TIP and wH-Me-O-TIP. With eye resolution, the color of the unaffected areas matches closely the color of wH-Me-TIP.

Film index	Color index	Changes after washing
wH-Me	0.70	intact film, with partial (medium) discoloration
wH-Me-P	0.05	intact film, with *complete* discoloration
wH-Me-O	0.08	intact film, with *complete* discoloration
wH-Me-TIP	0.90	intact film, with small discoloration
wH-Me-P-TIP	–	*cracked* film, with small discoloration
wH-Me-O-TIP	–	*destroyed* film, with parts completely removed and remaining 'islands' of material showing small discoloration

Figure 1. Modifications in the film appearance after washings with water/acetone. (See text for details). The samples shown are: (A) wH-Me-TIP, (B) wH-Me-P-TIP and (C) wH-Me-O-TIP.

observed after washing are summarized in Table 2. Few relevant images of the films' appearance after treatment with the above-mentioned solvents are shown in Fig. 1. To provide a reference for clean glass transparency, a small area (lower right corner) was removed from the initial H-Me-TIP (unwashed sample A) by mechanical means. All other modifications observed on the samples B and C are due only to the treatment with solvents. For samples A and C, the more colorful part (in the right side) of the films corresponds with a region were no solvent has touched the initial ormosil film. Since close to the edges of the glass slides, the thickness of the hybrid films has also an increase, the zones chosen for measurements of the color index were located in the middle of the samples (where the thickness variation was always below 10%). The cracks developed on wH-Me-P-TIP give a slightly opaque appearance of the sample B in Fig. 1. For wH-Me-O-TIP, material removal due to solvent attack leaves macroscopic-sized areas free of ormosil/dye (see the transparent regions of sample C). None of these effects was seen on wH-Me-TIP.

Since the general features observed using AFM were similar for a given recipe, with and without Rh-B, we resume ourselves to present only the data obtained on the Rh-B_doped materials. In order to avoid confusion, the "washed" samples are identified by an extra letter. For example, wH-Me-O indicates a composite film prepared according to the recipe in Table 1 from MeTES/OTES with rhodamine B and having a surface washed (with water/acetone).

Film Topography (Contact Mode AFM) and Inner Structure (TEM/cryo-TEM)

Films Made from Silica-Derivatives. The AFM image taken on the initial, *as dried*, H-Me composite (Fig. 2(a)) shows a nonflat relief, with small sized entities protruding out from the film. A zoom image (not shown here) around the hole (the black region) shows that the structure of the material consists of granules. Transmission electron microscopy (TEM) images (Fig. 3(a)) on the non-dyed H-Me ormosil sample confirm the existence of granules with relative smooth surface. After doping with rhodamine B and casting/drying the initial sol into a film, the granules are packed in a compact structure, with no obvious voids between them (see Fig. 2(a)). The space between these primary particles seems to be filled. Most probably, this "filling material" consists from rhodamine B and, perhaps, some partially-reacted compounds (siloxanic oligomers), unable to organize themselves in particles.

HRTEM micrographs (data not shown) did not provide conclusive evidence for the siloxanic oligomers. However, the drying procedure applied in samples' preparation (for TEM) could have forced these small-order chains/structures to attach/colapse on the surface of the granules.

Washing the film surface of the dyed H-Me film with water and acetone stimulates partial dissolution of the filling material. Hence, the topography (see the AFM image in Fig. 2(b)) shows more clear the granular structure together with 'islands' where material removal is not completed. Partial (small, but still detectable with eye resolution) discoloration of the film suggests that some rhodamine is also removed from the composite. These findings suggest that the granular structure

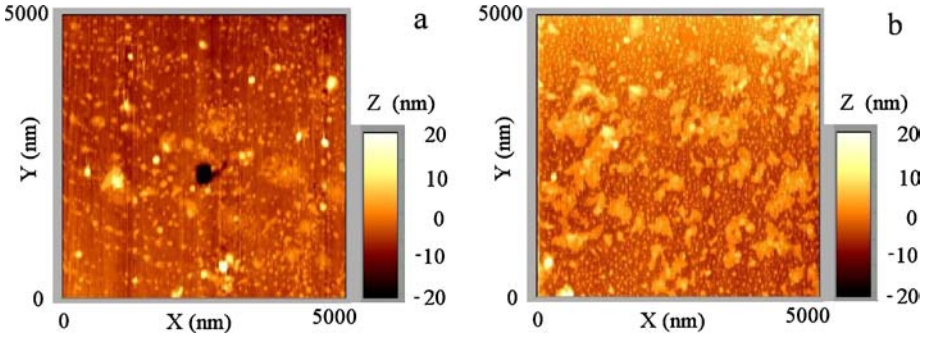

Figure 2. AFM height images acquired in *contact mode* (constant force 5 nN) on the surface of the H-Me (a) and wH-Me (b) films. The images were recorded while scanning on a (5×5 μm^2) area.

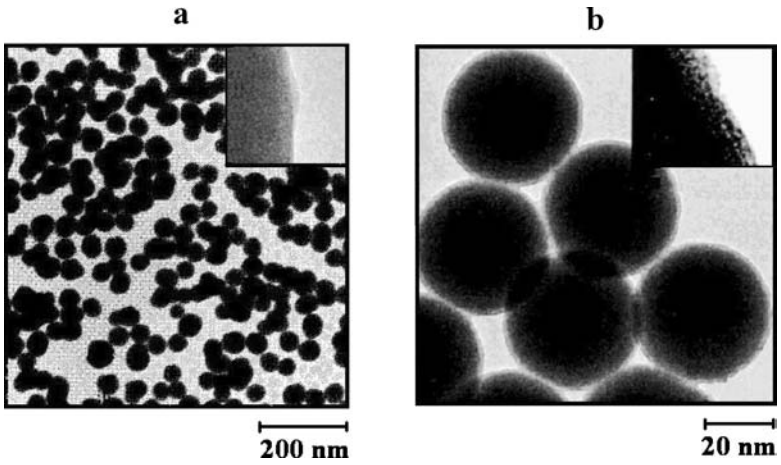

Figure 3. TEM micrographs showing the granules (particles) specific to H-Me (a) and H-Me-TIP (b) ormosils without dye. The inserts (upper left in both images) are HRTEM images.

protects the dye trapped in the bulk (i.e., between the particles) of the H–Me material and the water/organic solvent removes only the Rh-B from the superficial layer of the film.

Adding the phenyl compound to the preparation recipe increases the inhomogeneity in the film (Fig. 4(a)). The non-granular compounds are more easy removed by water/acetone (Fig. 4(b), compared with Fig. 2(b)).

Combining the results of cryo-TEM (Fig. 5(a) and (b)) and AFM imaging (Fig. 6) proofs that the H-Me-O hybrid undergoes structural changes during the transition from the initial liquid sol to the solid ormosil film. In order to inspect closer these changes in relation with different stages during film formation, dye-free H-Me-O sols were subjected to cryo-TEM. After examination of the vitrified state, the same samples were investigated also after an additional treatment. Namely, the frozen samples were withdrawn from the measuring chamber, allowed to warm up slowly and dried under mild vacuum. The final step was to re-visualize the completely dried samples.

A large proportion of the material in the initial H-Me-O sols is non-granular (light grey areas in Fig. 5(a)). Aging and solvent evaporation from the as-prepared hybrid phases, in mild thermal conditions, permits the reorganisation of the material into pseudo-granules and aggregates of the latter (see Figs. 5(b) and 6). In the AFM images (see an example in Fig. 6), large clusters of spherical entities are clearly visible on the initial ormosil film and large pores separate these agglomerated structures. It may be that enhanced hydrophobic interactions act as a 'liant' for (also inside) these pseudo-granules. After washing, the clusters could not be

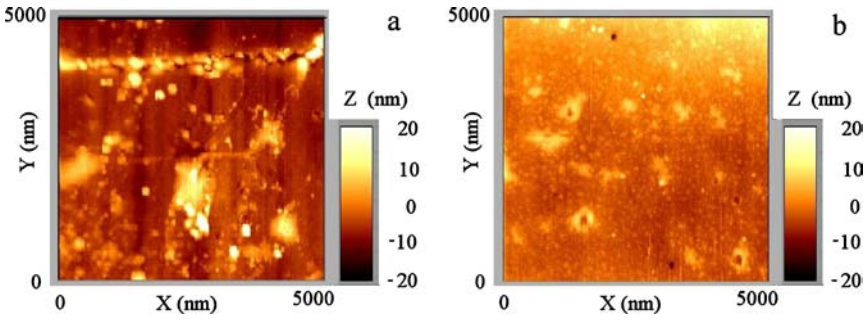

Figure 4. Surface topography of the H-Me-P (a) and wH-Me-P (b) films. Same conditions as in figure 1 were used for the AFM scanning.

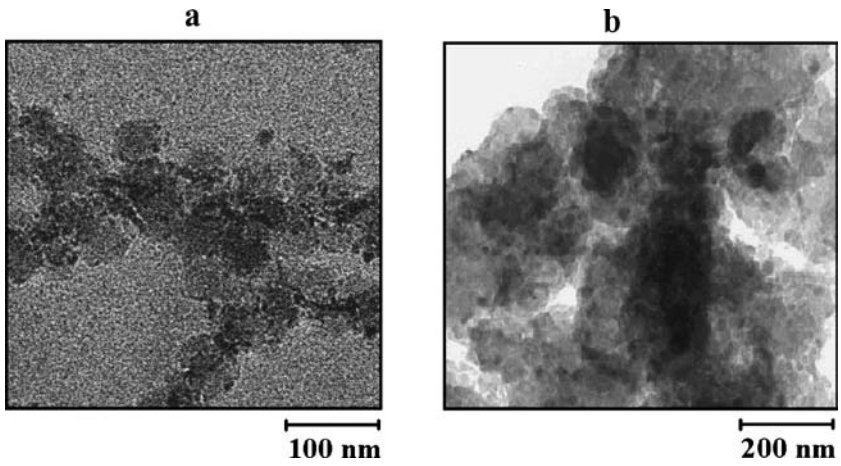

Figure 5. Micrographs obtained using cryo-TEM on a sample prepared from the H-Me-O sol in the vitrified state (a) and after drying (b). (See the text for details).

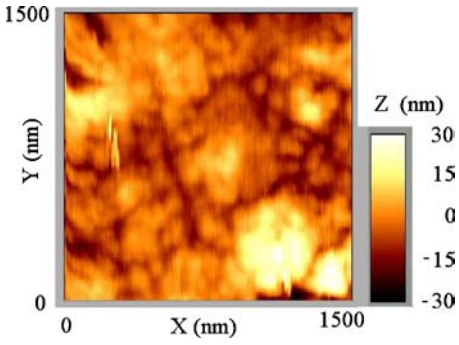

Figure 6. Image of the H-Me-O film as resolved using the contact mode AFM.

distinguished anymore on the topographical images. We incline to attribute this to film restructuring; the material that was initially entrapped becomes more mobile when swelled with solvent. This favors material reorientation, even pseudo-granules' partial or total dissolution. Subsequent drying of the wH-Me-O film would result in film topography with less resolvable features.

Using (TIP-MA) in Composite Films Synthesis. For the H-Me-TIP hybrid, compact and relative uniform (in size) particles are clearly present in the initial sol (Fig. 3(b)). As result of the titania precursor/MA addition in the formulation of H-Me-TIP, the roughness of these particles has a clear increase (Fig. 3(b) compared with Fig. 3(a)). Contact mode AFM images (Fig. 7) show that similar particles are present also at the film surface even for the non-washed hybrid. For films containing Rh-B, the washing procedure does not change the dimension of the granules (average diameter around 46 nm), but slightly fills the space between them with dissolved (or swollen) material. As a result, the top_film topography is almost unchanged. Compared with wH-Me, the wH-Me-TIP composite contains a larger Rh-B

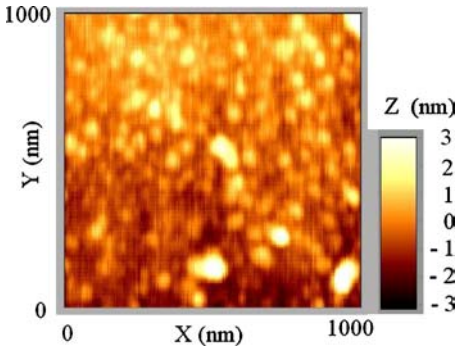

Figure 7. High resolution AFM height image on the surface of the H-Me-TIP film.

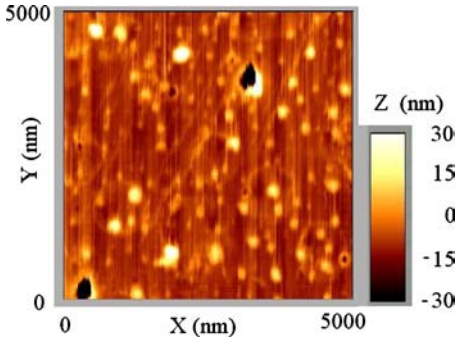

Figure 8. Structure of the H-Me-O-TIP film.

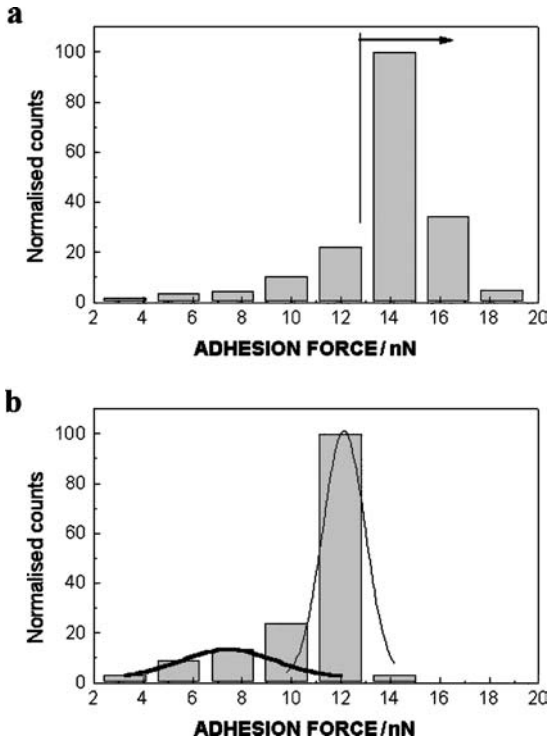

Figure 9. Force histograms of the tip-sample adhesive forces experienced on retracting the tip from the surface of the H-Me hybrid film. The sample was examined after 30 min (a) and after 3 h (b) in air. The experimental data were normalized to the value of the dominant component (in terms of counts).

amount (Table 2). Change of the hydrophobic moiety of the *tri*ethoxysilane used in synthesis (from MeTES to PTES or OTES), coupled with addition of the titania compound, has a drastic effect on the internal structure of the hybrid films. While the holes in the H-Me film (Fig. 2(a)) are extremely rare (as proved by extensive scanning along the surface), the H-Me-O-TIP film is very irregular (Fig. 8), with many holes, granular humps (clusters) and a high amount of 'filling' material. The large number of holes (for H-Me-O-TIP), together with a more porous structure of the material (for both formulations containing the more hydrophobe silica derivatives, i.e., PTES and OTES) are in good agreement with the observed damages of the film integrity (Table 2, Fig. 1) on the washed products.

Results After Force_Versus_Distance (3D_AFM) Experiments. Preparing the samples for 3D_AFM measurements, for all ormosils, the film surface was initially flushed with a very strong nitrogen stream for 15 min. By this treatment, all impurities (i.e., which are not strong, chemically, attached to the material) are removed. Leaving the film in air (relative humidity 60%) for 30 min, water starts to adsorb at the surface. Hence, the histogram of the measured adhesion forces shows, besides the tip-sample interactions, a major contribution coming from the growing water clusters (see Fig. 9(a), the values higher than 14 nN). If the composite is kept in air for another 3 hours, the adsorbed water layer grows as high as 6 microns on the top of the film. The thickness of the water layer was measured also via AFM. In the follow up 3D_AFM recordings, the ramping amplitude of the piezo tube was set as to measure only the tip–film interaction as mediated via the water layer. In this case, the contribution coming from capillary water adhesion is eliminated (Fig. 9(b)).

The silicone nitride tip is polar and, in the force histograms, the polar–polar interactions will be reflected in higher adhesion forces compared with (tip) polar–nonpolar (sample) interactions.

Two populations, with different polarities, contribute to the force histogram (Fig. 9(b)) for H-Me. The second

Table 3. Influence of washing (water/acetone) on the adhesive forces experienced on retracting the AFM tip from the surface of a composite (hybrid) film. Force histograms calculated based on 3D_AFM data.

Product synthesized with	Initial	After washing
MeTES	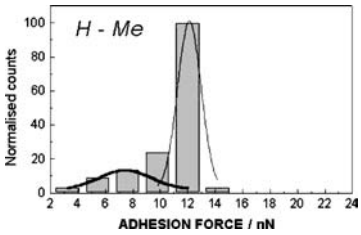	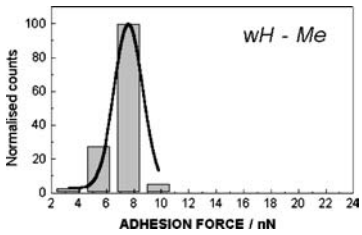
MeTES/PTES	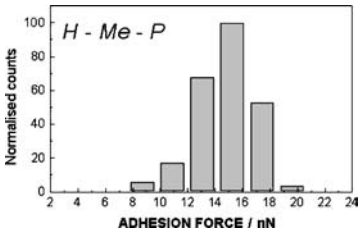	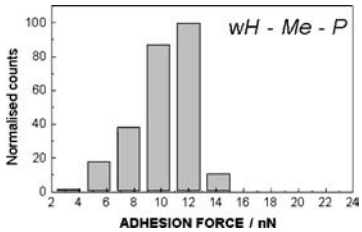
MeTES/OTES	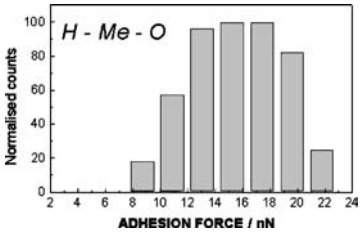	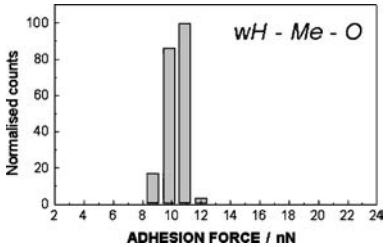
MeTES and TIP/MA	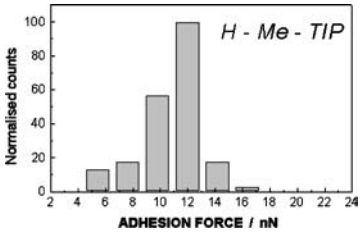	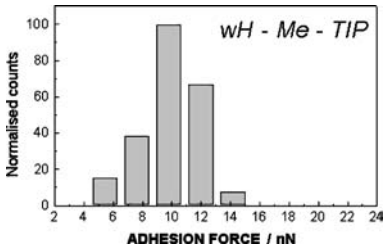

peak disappears after washing (Table 3), in agreement with the observed material removal (Fig. 2(b)). The dye and partially reacted material in the top layer (Table 3, initial H-Me) are more polar than the remaining material. A smaller adhesion between this latter and the AFM tip (Table 3, wH-Me) could be generated by a relative high incidence of the CH_3–groups covering the inorganic spheres.

The pronounced polar character for the surface of H-Me-P decreases considerably after washing. The entire force histogram moves toward lower values.

At the first look, for the hybrid prepared with OTES, the 3D_AFM data (see H-Me-O in Table 3) seem peculiar; these data can be explained only based on samples' topography (Fig. 6) and behavior after washing. The wH-Me-O film has an identical force histogram (of the adhesion forces) as a reference film, prepared from pure TEOS and subjected to the same washing procedure. Such observation points toward a solvent-induced film restructuration, where the top-layer after drying has only hydroxyls and Si-O-Si patches at the air/solid interface. For H-Me-O composite, the *force_versus_distance* measurements are influenced by the superficial structure of the film (Fig.6). Compression of the AFM tip into a flat (or almost flat) surface, up to a well-defined force setpoint (as in our

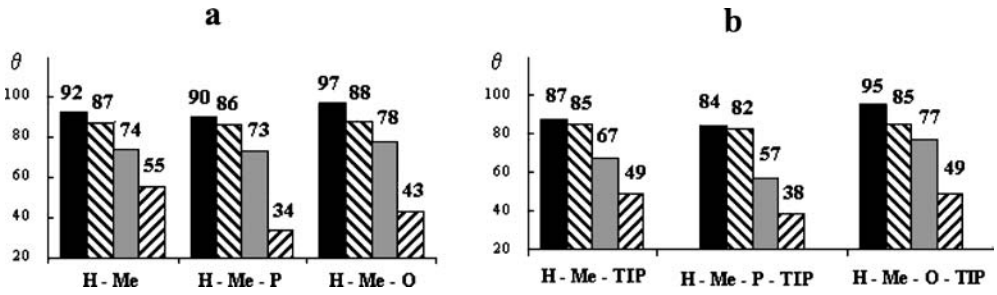

Figure 10. Average values for the contact angles (θ) of different liquids at the surface of films prepared without (a) and with TIP/MA (b). All data correspond to dye-doped preparations. The liquids used were: water (black), glycerol (strips right), ethylene glycol (grey) and α-bromonaphtalene (strips left).

experiments) is characterized by extremely small variations of the (tip-sample) contact area. Performing the measurements in identical conditions for a high irregular topography (like H-Me-O cluster-like film), the tip-sample contact area has a substantial increase. Because it is not a smooth contact, correct estimation of this area is impossible. We can observe though its consequences, as an artificial broadening of the adhesion force histogram and shifting towards higher values (Table 3). In this respect, the H-Me-O hybrid is not more polar than H-Me or H-Me-P, but we have no means to determine from 3D_AFM the correct values for H-Me-O polarity.

The almost identical topography of H-Me-TIP and wH-Me-TIP gives minor differences in the force histograms (Table 3). The initial H-Me-TIP film has the characteristics of a patched surface made from a less polar component (like the one measured for wH-Me) and a pure inorganic, polar material.

When probing the adhesion on pure titania particles, an average normalized force of 0.3 nN per nm was obtained (see Fig. 9 in reference [33]). (We have used here the term "normalized" as to define the adhesion force divided by the particle diameter: $F_{\text{normalized}} = F_{\text{adhesion}}/D_{\text{particle}}$). Calculation of the $F_{\text{normalized}}$ for the polar patches of H-Me-TIP and wH-Me-TIP give comparable values. These findings are in line with a particle structure where the surface has zones of TiO_2 or Ti-O-Si rich composition.

Hybrid Wettability

While atomic force microscopy offers information on small length scale, the contact angles and surface energies values (as determined via the wetability studies, Fig. 10(a)–(b) and Table 4) give an average over the film superficial properties at the macroscale. The Lifshitz-van der Waals (γ_L^{LW}) surface energy is related with the interaction between the film components as manifested at the solid/air interface. Meanwhile, the acid-base (γ_L^+ *and* γ_L^-) contributions indicate the surface character as electron acceptor or, respective, donor.

The films dried from non-dyed composites with PTES or OTES have a pronounced monopolar character (no or extremely small γ^{AB}). On average, TIP/MA addition gives an increased electron donor character (higher γ^-). The only exception is the H-Me hybrid.

Table 4. The surface energy components (mJ m^{-2}) of hybrid films.

	WITHOUT Rh-B					WITH Rh-B				
Film index	γ^{LW}	γ^+	γ^-	γ^{AB*}	γ^{tot}	γ^{LW}	γ^+	γ^-	γ^{AB*}	γ^{tot}
H–Me	28.346	0.11	2.121	0.966	29.312	26.341	0.193	4.021	1.761	28.102
H–Me–P	37.303	0	0.463	0	37.303	36.158	0	1.143	0	36.158
H–Me–O	31.776	0.004	0.052	0.029	31.805	30.449	0.023	0.31	0.168	30.617
H–Me–TIP	30.252	0.015	1.066	0.253	30.505	29.333	0.007	5.748	0.401	29.734
H–Me–P–TIP	37.267	0.001	1.173	0.068	37.335	35.742	0.079	1.505	0.583	36.326
H–Me–O–TIP	32.747	0.001	0.332	0.036	32.783	31.071	0	1.798	0	31.071

All films with Rh-B show an even higher shift towards electron-donor species in the superficial layer (i.e., higher γ^- than the ones measured on films without the dye).

The titania presence has only a minor influence on the mutual interactions between the film constituents at the hybrid surface. Hence, γ_L^{LW} values are slightly modified for similar recipes with TIP as compared with formulations without it. Quite interesting is that all PTES-based hybrids have higher γ_L^{LW} values, most probably generated by the interaction between the phenyl ring of the precursor and the hydroxyls of the inorganic matrix. Also, these hybrids (with PTES) give the smallest dispersion of the contact angle data (results not shown).

The wettability data are in very good agreement with the results obtained using 2D (*imaging*) and 3D_AFM. While washing the films only with water, no changes were observed (visual) or measured (AFM, contact angle measurements), subsequent washing with acetone induces modifications, detectable with both methods. For H-Me, the value of the contact angle with water increases, from 92 (nonwashed sample) to 97 (washed sample) which confirms the AFM results: a higher contribution of the nonpolar groups (CH_3-) at the film surface (wH-ME, in Table 3) and a slight rugosity increase (Fig. 2(b) compared with Fig. 2(a)). The pronounced polar character of H-Me-P (which gives the smallest θ value for water: $\theta_{w/\,H-Me-P} = 90$, see Fig. 10(a)) decreases after washing ($\theta_{w/\,wH-Me-P} = 81$). This effect is based on a higher contribution of the polar species in the surface region and a relative uniform material distribution (Fig. 4(b)). In consequence, for H-Me-P, hysteresis of the contact angle values is completely absent.

Thermogravimetric Analysis

TGA measurements provide information about the thermal stability and reflect the bulk properties of the end materials produced via the sol–gel method.

The H-Me composite has a diffuse thermal degradation (Fig. 11), very much alike the one specific for pure silica. The first weight loss (from low temperatures up to 120°C) is very small (below 1%) and indicates water evaporation from the, apparent, hydrophobe hybrid. The CH_3–silica network linkages are degraded by higher temperatures, above 200°C.

In comparison, the TGA curve for H-Me-TIP (Fig. 11) has two additional features. The first one is related with the thermal degradation at heating up to 200°C. In this temperature range, besides more ('superficial") water loss (2.5%), the film looses as well the water, solvent and perhaps other organic groups produced during condensation reaction, all entrapped in the pores of the composite. The titania derivative contributes in building up this porous structure of the H-Me-TIP particles. The second feature refers to the double-step weight loss observed between 450°–550°C. As reported by Khalil and coworkers [32], individual small particles with a high titania content can aggregate into bigger structures, preceding the transformation to anatase. It is not excluded that such a process is accompanied by exposure of new areas from the silica-rich particles. Hence, the superficial CH_3—SiO_2 and/or CH_3—TiO_2 bonds, formerly 'protected' by the external titania spheres, will start to degrade.

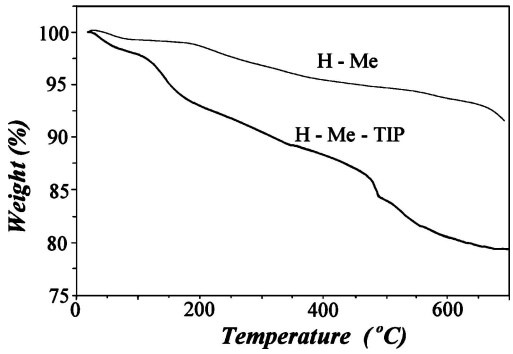

Figure 11. TGA curves obtained for MeTES_based composites, with and without TIP/MA .

Denoting a very hydrophobic character, no evaporation of water/solvent is present before the major degradation peak (Fig. 12(a)) measured for H-Me-O. The latter starts at 250 °C and ends at 400°C. The temperature range is specific for hydrocarbon chains and indicates scission of the octyl groups. The derivative thermogravimetric (DTG) curve shows also the small peak for methyl degradation. Good agreement between the calculated and measured weight losses confirms that the hydrolysis/condensation reaction is complete for both H-Me and H-Me-O. In these circumstances, the 'filling' material of H-Me (see AFM images, Fig. 2(a)–(b)) must be small-order oxidic chains/networks including in their structure CH_3- groups. Meanwhile, the octyl-enriched recipe (used for H-Me-O) is likely to generate a higher amount of the oligomeric siloxanes (as confirmed via cryo-TEM, see Fig. 5(a)). Since their structure is decorated with C_8H_{17}, a higher tendency for hydrophobic interactions will generate granular-like

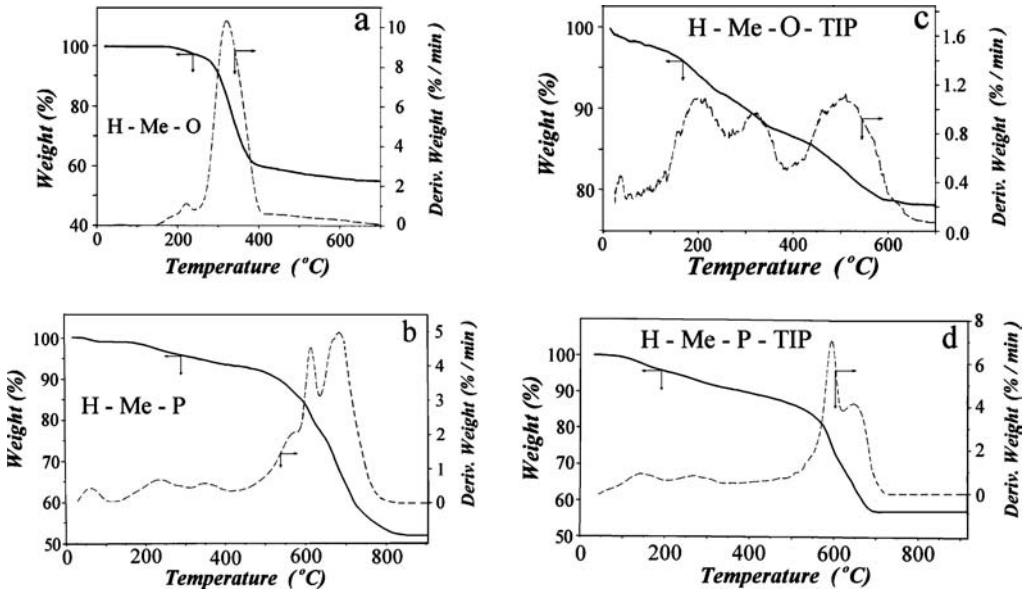

Figure 12. TGA and DTG (dashed) curves for hydrophobic-rich composite films.

assemblies (pseudo-particles and clusters) as observed by cyo-TEM (Fig. 5(b)) and AFM (Fig. 6), with organic-rich nanodomains.

The structure of H-Me-P is even more complex and its thermal degradation curves (Fig. 12(b)) help us only partial to understand it. A porous (i.e., more porous than H-Me) and relatively polar (i.e., more polar than H-Me-O) structure keeps inside the volatile components, which are released or degraded below 400°C. The material weight loss is 7% when this heating temperature is reached. Further on, the degradation of the composite involves structure collapse, with burning of the former 'protected' organics. The initial organization in the H-Me-P does not originate from a *single population*-building blocks, thus the measured multi-peak aspect of the DTG curve in Fig. 12(b).

The additional features already discussed in the analysis of the TGA curve of H-Me-TIP are also present for composites prepared with addition of the more hydrophobic precursors (i.e., OTES and PTES) and TIP/MA (Fig. 12(c) and (d)). They are superimposed on the thermal degradation curve of the respective composite without titania. Again, a higher retention of water/organics and structural changes (above 400°C), tell us that the starting materials (H-Me-O-TIP and H-Me-P-TIP) are porous and extremely inhomogeneous (in terms of their 'primary' species).

Spectral (Absorption/Fluorescence) Data

Rhodamine B (Rh-B) belongs to the class of xanthene dyes, whose optical properties depends on many factors, such as solvents (polarity and aprotic character), concentration, pH value, etc. [34–36]. Generally, it has three molecular forms (Fig. 13). For our samples, the sol–gel reaction was conducted in acidic conditions. Moreover, the addition of MA slightly increases the acidity. (In the preparative conditions of our recipes, this organic monomer has an acidic character.) According to literature data [22, 36], in these conditions, the equilibrium between the zwitterionic and cationic forms (i.e., the only colored species of the dye) is shifted towards the latter. In polar solvents (such as ethanol), the carboxyl groups participate in a typical acid–base equilibrium: $RBH^+ = RB^{\pm} + H^+$.

It is known that absorption/emission spectra for fluorescent dyes are sensitive to the local microenvironment encapsulating and/or interacting directly with the dye molecules [13, 15, 16, 19, 20]. Since the interest in preparing RhB-doped materials is related with future applications in the field of solid-state lasers, we begin by presenting the results of the emission fluorescence spectral analysis. Further on, to relate our data with the possible guest (dye)—host (matrix) and/or guest-guest interactions, we comment on the information extracted from the absorption spectra.

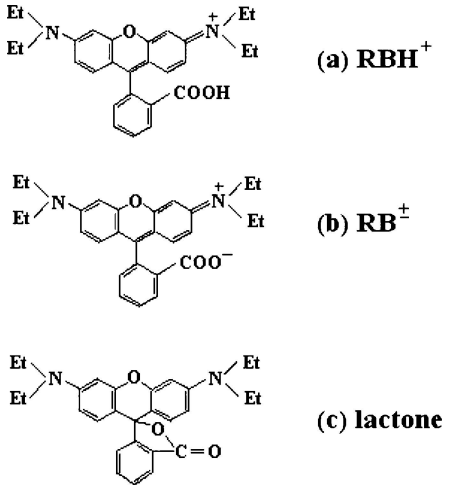

Figure 13. Structural forms of rhodamine B. The (a) and (b) forms are strongly colored and emissive. The lactone form (c) is colorless and shows no emission because the π-electron system of the dye chromophore is interrupted. Its formation is also stimulated by high temperature treatment of the (a) and (b) forms.

As a general observation, for the investigated films with Rh-B, the emission fluorescence spectra show similar characteristics with those obtained for Rh-B_doped silica [18]. No doubt, TIP presence in the composites modifies the nature of the inorganic matrix and affects the interaction with the added dye. The measured emission band (see Fig. 14(b)) results from the electronic transitions of the rhodamine B monomer. This transition involves a change from the vibrationally lowest-lying level of the first excited electronic state S_1 to the vibrationally excited sublevels of the electronic ground state [23]. The glassy matrix (generated via the sol–gel process) is not expected to change much upon addition of the dye, but the number of dye molecules that are in each others vicinity as well as the dye—matrix interactions could be different, making very difficult to assess the results in terms of a single effect. When the number of Rh-B molecules in a given domain increases, the interaction between neighboring dye molecules is enhanced. This effect lowers their excited state energy and produces a red shift in the spectra, as observed previously [37] Secondly, a self-absorption process could also be responsible for small red shifts in the emission band. The more concentrated in Rh-B is a sample, the larger is the red shift of the emission band. Also, interactions between Rh-B and the phenyl rings of PTES (i.e., π–π interactions [38]) are not excluded and are expected to generate a similar shift towards larger wavelengths.

The wavelength (around 580 nm) of the peak characteristic for the fluorescence emission spectra of the dye-doped hybrids confirm that Rh-B exists in the cationic form (variant (b) in Fig. 13) in these composites [22, 36]. Blue shift of the peak positions (from 588 nm towards 560 nm) could be an indication for the decrease in Rh-B cationic species and formation of new species at the expense of this cation. In dye doped solids, highly acidic cage environment is capable to supply more protons (H^+) to rhodamine-B cation. These (H^+) ions are attached to the nitrogen atom (uncharged) carrying a lone pair of electron in the structure of Rh-B cation resulting higher protonated form. Due to Coulombic repulsive interactions, the attachment of H^+ ion at the nitrogen atom carrying positive charge is not possible. Thus, a higher protonated form of Rh-B induces a blue shift in the fluorescence peak of the dye in the hybrid films. The balance between the cation form and higher protonated forms of Rh-B could explain (at least

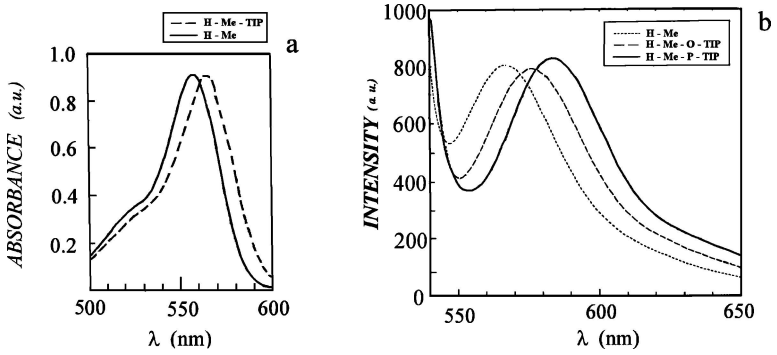

Figure 14. Absorbance (a) and Emission fluorescence (b) spectra measured on selected composites. The shifts in the wavelength (λ_{max}) of the peaks give information on the local interactions (see the text for details).

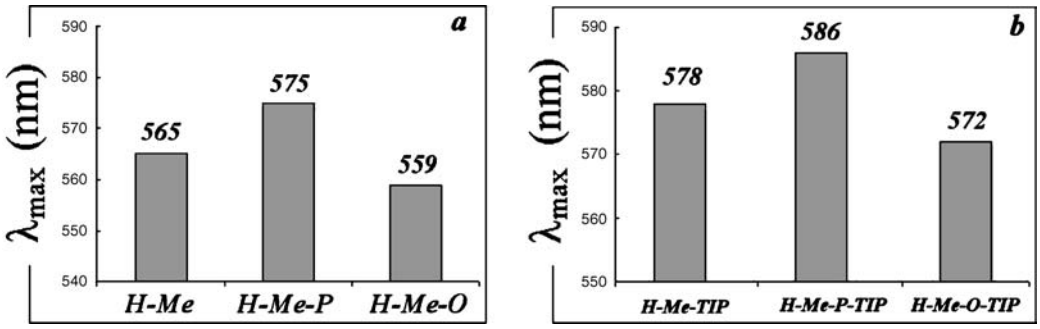

Figure 15. Changes of the wavelength of the emission peak (λ_{max}) for fluorescence spectra of rhodamine B –doped hybrids, as function of composition, without (a) and with TIP/MA (b).

partial) the different λ_{max} values obtained for the fluorescence peaks of the composites (Figs. 14(b). and 15).

The first comment than can be made while looking at the emission peak values (in Fig. 15(a)–(b)) is that the wavelength of the maximum is smaller for hybrids (with similar RTES) without TIP/MA. A similar phenomenon was observed for molecularly doped (with Rh-B) SiO_2/TiO_2 hybrids [24]; as the TiO_2/SiO_2 ratio was increased, the orange emission bands (corresponding to the spontaneous fluorescence of rhodamine B) have a shift towards higher wavelengths. In our recipe, the almost constant wavelength red shift ($\Delta\lambda_{max} \cong 11 \div 13$ nm) of the films prepared from a given alkoxysilane(s) with TIP/MA (Fig. 15(b)) as compared with the similar one without these additives (Fig. 15(a)) is generated by a higher polarity of the titanium-incorporating silica structures. (We would like to remind the reader that, at the moment of RhB addition in the samples prepared only with silicium compounds, the dye molecules will encounter not *pure* silica structures, but rather species with (at least partial) screening of the polar parts. This screening is due to the presence of the hydrophobic moieties and could be more or less advanced. Meanwhile, for the TIP/MA-rich recipes, the TiO_2 polarity suffers less from this drawback.)

In order to check if the observed trends in the fluorescence emission spectra are artifacts generated by a different concentration of the dye in the films, we prepared and analyzed (both by fluorescence and absorption) other two series of films:

(i) samples having a double concentration of RhB, but the same thickness as the *standard* films (i.e., the 30 μm thick films which were used for the complete set of analyses along the article), and

(ii) films with different thicknesses (up to 100 μm), cast from the initial recipes.

If dye concentration or film thickness increase, the emission peaks have a red shift of maximum 4 nm, while the absorption peaks show only modification of the intensity but not of the λ_{max}. These results are in perfect agreement with earlier reported data [21, 23].

All the absorption spectra (see two examples in Fig.14(a) for the standard films) have an intense peak (specific to the monomer of RhB) at 560 nm, which is neighbored by a shoulder at smaller wavelength ($\sim$ 525 nm, attributed to the RhB-dimer). The monomer-dimer ratio was found to be independent on the recipe, which means that none of the formulations has an enhanced aggregation of the dye. Meanwhile, the absorption peaks show roughly the same trend as the emission spectra: for a given precursors composition, the film with TIP has an average red shift of $\Delta\lambda^{abs}_{max} \cong 10 \div 12$ nm when compared with λ^{abs}_{max} of the titanium-free film.

The complete spectral analysis allows us to conclude that it is not the difference in dye concentration or an aggregation process that manifest themselves in the spectra. Enhanced (dye-matrix) interactions and polarity in TIP preparations are responsible for the observed shifts of the spectra (Fig. 14(a)–(b) and 15 (a)–(b)). These guest-host interactions are present not only at air/composite surfaces (as proved by the wettability studies), but also in the bulk of the films (see the results of this section). Additionaly, the data in Fig. 15 also point towards the idea that MeTES/PTES hybrids have enhanced dye-(PTES) phenyl ring interactions.

Further Comments on Dye Retention

If ormosil materials are designed/prepared to be used in real-life applications, the end product must be able

to keep the same structure/properties over long time periods. In this respect, one major requirement is that none or insignificant modifications are generated by treatment with mild solvents. As already summarised in Table 2, some of the formulations studied by us do not meet the required standard: (a) some of the ormosil films show partial or even complete lost of Rh-B after washing with water/acetone, (b) other films show major changes in the structure/film integrity.

To evaluate if the solvents used remove only the dye or also part from the matrix, we have recorded the FTIR spectra of the dried samples prior as well as after washings. The assignment of the absorption bands was done in accordance with published literature data [25, 32, 39–43]. Figure 16 shows few relevant spectra.

The spectra in Fig. 16 were selected because not only that they show spectral contributions from all compounds, but also easy distinction between the separate contributions can be done, making the data interpretation more accessible to the reader.

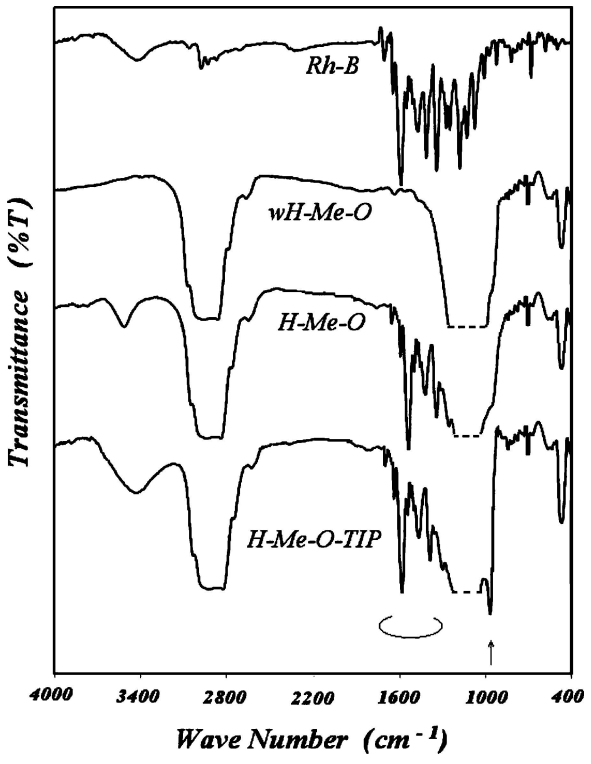

Figure 16. FTIR spectra of octyl-containing ormosils. (See text for details). The absorption bands in the spectral region specific for the inorganic Si-O-Si (i.e., between 1250 – 1000 cm^{-1}) are very intense; hence, the peaks are partially not plotted (the dotted line zone). For comparison purpose, the spectrum of the dye (Rh-B) was also included.

For all ormosils, the Si-O-Si groups give a strong absorption band in the spectral region between 1250–1000 cm^{-1} (asymmetric stretching and a small contribution from the longitudinal optical component of the high-frequency vibration of SiO_2). Additionally, the other vibrational modes of Si-O-Si bonds are present in the spectra: the symmetric stretching ($\sim$750 cm^{-1}) and the transverse rocking ($\sim$460 cm^{-1}). For formulations with TIP, a clear peak at $\sim$960 cm^{-1} (pointed by the arrow in Fig. 16) indicates the existence of Si-O-Ti linkages. A strong band located between 3000 and 2800 cm^{-1} corresponds to the CH_2- symmetric stretching. Compared with this contribution assigned to the octyl chains, the absorption peaks for the terminal -CH_3 or for the phenyl ring in dyed H-Me or (respective) H-Me-P, with and without TIP, are screened by the multiple peaks of Rh-B (visible in Fig. 16 in the region 1700–1300 cm^{-1}). Washing the H-Me-O ormosil results in complete film discoloration; hence, the FTIR spectrum of wH-Me-O (in Fig.16) does not show anymore the presence of the dye. Same behavior was seen also for wH-Me-P.

Corroborating the data from FTIR spectroscopy with the observations after visual inspection of the films before and after treatment with solvent (see also Table 2 and Fig. 1), it seems that, for ormosils without TIP, only the dye is removed. Meanwhile, if TIP is used in the initial recipe, the composition of the removed material depends on the precursor(s) combination. Minor Rh-B removal and no ormosil modifications (in terms of composition) are manifested for wH-Me-TIP as compared with H-Me-TIP. Small decreases of both the amounts of dye and hybrid material were noticed for H-Me-P-TIP. The solvent attack is quite strong on the H-Me-O-TIP: massive changes in the film integrity (see sample C in Fig. 1 and the comments in Table 2) and a decrease of the Si-O-Ti peak (960 cm^{-1}) with respect to both organic (CH_2-) and inorganic (Si-O-Si) contributions in the FTIR spectrum (data not shown) indicate a preferential displacement of titanium-rich zones from the wH-Me-O-TIP. However, the remaining film retains some TiO_2. The exact amount of the titania compounds removed after washings cannot be estimated based only on FTIR data; the peaks belonging to the Ti-O-Ti vibrations are located in the 900–400 cm^{-1} range [43], where also the skeletal vibrations of the silica network are present. Based on available (FTIR) data, a phase separation (in organic-rich and polar-rich

zones) in the initial H-Me-O-TIP material cannot be excluded.

Conclusions

Complete review of the AFM, TEM and TGA data helps getting more insights in the actual structure of the hybrid films prepared from RTES (pure or with added titania compound) following the sol–gel route. When the starting precursor is pure MeTES, the reacted (via hydrolysis/condensation) product is organized in compact, non-porous spheres.

Enrichment of the preparation recipe with either PTES or OTES only generates a smaller reactivity in the system and more small-order oxidic structures (i.e., oligomeric siloxanes), unable to be incorporated in similar, high-order entities (*i.e.*, particles) The hydrophobicity increase stimulates the transition of film structure: from well-defined, compact particles (for H-Me), to a mixture of porous particles and non-granular material (for H-Me-P), with the extreme result observed for H-Me-O. For this latter, the apparent homogeneity comes from cluster-like organization, where the primary entities are likely to be *'pseudo—granules'* produced by hydrophobic interactions of the small-order oxides.

TGA data strongly support the idea of an even more complex material structure for titania containing recipes. The spherical 'core', formed during the first 2 hours of reaction from pure MeTES precursor, is decorated on the outside by a shell made either from pure titania particles, either from spheres with an interlinked three-dimensional network of TiO_4 tetrahedra and partial SiO_3 tetrahedra. These external spheres are too small to be seen even with AFM resolution, but their existence is proved by TEM (Fig. 3(b)) and TGA analysis (Fig. 11 and 12(c)–(d)). The resulting materials have more capacity for retention of solvent (i.e., water, ethanol) and suffer reorganization at heating above 400°C. Similar reaction paths (and results) happen as well for H-Me-O-TIP and H-Me-P-TIP. The biggest contribution of the titania-rich material is found for H-Me-P-TIP. Massive screening of the hydrophobe parts in the H-Me-O-TIP composite ends in a film structure completely different than H-Me-O, with no (or at least not high-dimensional) 'pseudo'-granules.

The resistance of the dye-doped materials against solvent-induced dissolution was checked by washing the films with water and acetone. On materials made only from silica-compounds, strong (up to total) discoloration of the composite films after washing with acetone indicates massive removal of the dye from the film. It seems that dye transport inside the inorganic structure is not facilitated when the composite recipe does not contain the TIP/MA combination. For such films, the dye is located in the macropores (between the granules) of the material and could be easy removed by washing. On the contrary, using TIP/MA apparently changes not only the internal composition of the granular-like material (by creating a microporous outer-shell of the particles) but also the affinity of the Rh-B to permeate and reside inside this new structure. Existence of more hydrophobic zones (or even domains), like in the case of H-Me-O, is not favorable for Rh-B incorporation. In fact, the long octyl chain has a detrimental effect on the film properties; the organic solvent destroys the film integrity (see Table 2 and Fig. 1, wH-Me-O-TIP), while removing only slightly the dye from it.

In all films, rhodamine B is entrapped in its cationic form, as proved by fluorescence emission spectra and wettability data. The structures created in titanium-containing films have enhanced dye-matrix interactions.

For future applications, the film dried from H-Me-TIP is the best candidate. This material has very good qualities in terms of regular structure, dye incorporation and retention, resistance against washing with solvent.

Acknowledgments

The authors like to thank Kees van der Werf and Martin Bennink for valuable technical support on the AFM instrument. Stelica Cioaca is kindly acknowledged for his help during preparation of the manuscript.

References

1. R. Reisfeld, R. Zusman, Y. Cohen, and M. Eyal, Chem. Phys. Lett. **147**, 142 (1988).
2. M. Guglielmi, P. Colombo, L. Mancinelli Degli Esposti, G.C. Righini, S. Pelli, and V. Rigato, J. Non-Cryst. Solids **147**, 641 (1992).
3. M. Canva, G.L. Sanx, P. Georges, A. Brun, F. Chaput, and J.P. Boilot, Opt. Lett. **17**, 218 (1992).
4. F. Bentivegna, M. Canva, P. Georges, A. Brun, F. Chaput, and J.P. Boilot, Appl. Phys. Lett. **62**, 1721 (1993).
5. M. Casalboni, R. Senesi, P. Prosposito, F.D. Matteis, and R. Pizzoferrato, Appl. Phys. Lett. **70**, 2969 (1997).
6. R. Reisfeld, E. Yariv, and H. Minti, Opt. Mater. **8**, 31 (1997).
7. G.H. Hsiue, R.H. Lee, and R.J. Jeng, Chem. Mater **9**, 883 (1997).

8. T. Suratwala, Z. Gardlund, K. Davidson, and R.H. Uhlmann, J. Sol-Gel Sci. Tech. **8**, 973 (1997).
9. J. Lenhart, J.H. Vanzanten, J.P. Dunkers, and R.S. Parnas, Langmuir **16**, 8145 (2000).
10. C.J. Brinker and G.W. Scherer, Sol-Gel Science: The Physics and Chemistry of Sol-Gel Processing (Academic Press, San Diego, 1990).
11. D. Avnir, S. Braun, and M. Ottolenghi, in Supramolecular Arhitecture: Synthetic Control in Thin Films and Solids, edited by T. Bein, ACS Symp. Ser. **499**, 1992, p. 389.
12. E.J.A. Pope, J. Sol-Gel Sci. Tech. **2**, 717 (1994).
13. N. Wttouck, F. De Schryver, and I. Snykers-Hendrickx, J.Sol-Gel Sci. Tech. **8**, 895 (1997).
14. H. Nakazumi, K. Makita, and R. Nagashiro, J. Sol-Gel Sci. Tech. **8**, 901 (1997).
15. L. Hou, B. Hoffman, M. Mennig, and H. Schmidt, J.Sol-Gel Sci. Tech. **2**, 635 (1994).
16. K. Mongey, J.G. Vos, B.D. Macraith, and C.M. McDonagh, J. Sol-Gel Sci. Tech. **8**, 979 (1997).
17. R. Litran, E. Blanco, M. Ramirez-del-Solar, and L. Esquivias, J. Sol-Gel Sci. Tech. **8**, 985 (1997).
18. J. Garcia, V.M. Castano, M.A. Mondragon, E. Ramirez, F. Gonzalez, A. Campero, and V. Renteria, J. Sol-Gel Sci. Tech. **8**, 911 (1997).
19. T. Schibata, M. Yamane, K. Kamada, K. Ohta, K. Sasaki, and H. Masuhara, J. Sol-Gel Sci.Tech. **8**, 959 (1997).
20. L. Matthews, D. Avnir, A. Modestov, S. Sampath, and O. Lev, J. Sol Gel Sci. Tech. **8**, 619 (1997).
21. X.M. Han, J. Lin, R.B. Xing, J. Fu, and S.B. Wang, Mater. Lett. **57**, 1355 (2003).
22. A.V. Deshpande and U. Kumar, J. Non-Cryst. Solids **306**, 149 (2002).
23. X. Hao, X. Fan, Z. Wang, and M. Wang, Mater. Lett. **51**, 245 (2001).
24. H. Yanagi, T. Hishiki, T. Tobitani, A. Otomo, and S. Mashiko, Chem. Phys. Lett. **292**, 332 (1998).
25. T. Seckin, A. Gultek, and S. Kartaca, Dyes and Pigments **56**, 51 (2003).
26. Y. Yang, M. Wang, G. Qian, Z. Wang, and X. Fan, Opt. Mat. **24**, 621 (2004).
27. K.O. van der Werf, C.A.J. Putman, B.G. de Grooth, F.B. Segerink, E.H. Schipper, N.F. van Hulst, and J. Greve, Rev. Sci. Instrum. **64**(10), 2892 (1993).
28. J.C. Berg in Wettability (Marcel Dekker Inc., New York, 1993), Chap. 2.
29. C.J. van Oss, R.J. Good, and N.K. Chaudhury, Langmuir **4**, 884 (1988).
30. M. Montes, F.P. Getton, M.S.W. Vong, and P.A. Sermon, J. Sol Gel Sci. Tech. **8**, 131 (1997).
31. R.M. Almeida and E.E. Christensen, J. Sol Gel Sci. Techn. **8**, 409 (1997).
32. K.M.S. Khalil, A.A. Elsamahy and M.S. Elanany, J. Coll. Interf. Sci. **249**, 359 (2002).
33. R. Jones, H.M. Pollock, and D. Geldart, A. Verlinden, Powder Tech. **132**(2-3), 196 (2003).
34. I. Lopez Arbeloa and P. Ruiz Ojeda, Chem. Phys. Lett. **79**, 47 (1981).
35. I. Lopez Arbeloa and K.K. Rohatgi-Mukherjee, Chem. Phys. Lett. **28**, 474 (1986).
36. D. Hinckley, P.G. Seybold, and D.P. Borris, Spectrochim. Acta **42A**, 747 (1986).
37. A. Imhof, M. Megens, J.J. Engelberts, D.T.N. de Lang, R. Sprik, and W.L. Vos, J. Phys. Chem. B **103**, 1408 (1999).
38. R. Tamaki and Y. Chujo, 37-th Int.Symp.Macromol., Gold Coast, Australia, Preprints, 1998, p. 278.
39. D.L. Ou and A.B. Seddon, J. Non-Cryst. Solids **210**, 187 (1997).
40. D.L. Ou and A.B. Seddon, J. Sol-Gel Sci. Tech. **8**, 139 (1997).
41. W. Que, Z. Sun, Y. Zhou, Y.L. Lam, Y.C. Chan and C.H. Kam, Thin Sol. Films **359**, 177 (2000).
42. L. Frunza,, H. Kosslick, U. Bentrup,I. Pitsch, R. Fricke, S. Frunza and A. Schonhals, J. Mol. Struct. **651–653**, 341 (2003).
43. P. Madhu Kumar, S. Badrinarayanan, and M. Sastry, Thin Sol.Films **358**, 122 (2000).